ADVANCED MATERIALS
www.advmat.de

Rewritable Optical Memory Through High-Registry Orthogonal Upconversion

Kezhi Zheng, Sanyang Han, Xiao Zeng, Yiming Wu, Shuyan Song, Hongjie Zhang, and Xiaogang Liu**

An experimental design, based on a combination of core–shell-structured upconversion nanoparticles and diarylethene photochromic molecules, for achieving rewritable optical memory is reported. This core–shell design enables the nanoparticles to emit two sets of distinct emission bands with ultrahigh spectral purity through laser excitation at 980 and 1532 nm. Importantly, the ultraviolet emission of the nanoparticles under 980 nm irradiation is used to activate the cyclization reaction of diarylethene through C—C bond formation, while the green emission from the nanoparticles upon 1532 nm excitation leads to the cleavage of the newly formed C—C bond. This pathway offers a convenient and versatile optical method for controlling the process of data writing and erasing with high spatiotemporal resolution.

In recent years considerable attention has been paid to photochromic materials due to their potential applications in molecular electronics and photonic devices.[1–4] As one of the most promising photochromic molecules, diarylethene molecules have been widely used for data storage and molecular photoswitching because of their short response time, high photoisomerization quantum yield, and outstanding fatigue resistance.[5–8] However, current diarylethene-based photoresponsive systems generally require the use of short-wavelength ultraviolet (UV) or visible light to trigger molecular isomerization, which may cause deleterious effects associated with low-density data storage and the cross-talk between multiple memory layers.[9–13]

Lanthanide-doped upconversion nanoparticles (UCNPs), which can turn near-infrared (NIR) excitation into visible or UV light emission, may provide a much needed solution to the above-mentioned problem.[14–23] Over the past few years, UCNPs and diarylethene-based molecules have been combined for nondestructive optical memory and photoswitching applications.[24–32] Despite the enticing prospect, these demonstrations are constrained by a number of limitations such as complex procedure, slow rates of photoreaction, and the inherent deficiency in data processing due to uncontrolled manipulation of ring-opening and ring-closing reactions of the diarylethene molecules. To this regard, we reason that a dual-channel orthogonal pumping scheme with 980 and 1532 nm lasers, by which the UV and green emissions of lanthanide dopants can be upconverted selectively on a single-particle level, would make rewritable data storage possible. Importantly, in contrast to the previously reported 800/980 nm excitation systems,[33–38] our design provides a precise control over the excitation of different activators, thereby offering the possibility of improving the spectral purity of orthogonal emission. As a result, a reversible photochemical reaction through remote NIR light activation can be readily implemented.

Herein, we demonstrate a facile, two-way photoswitching of DTE molecules (DTE: 1,2-Bis(2,4-dimethyl-5-phenyl-3-thienyl)-3,3,4,4,5,5-hexafluoro-1-cyclopentene) using core–shell structured upconversion nanoparticles that are excitable by both 980 and 1532 nm lasers (**Figure 1**a). In a typical experiment, multilayer $NaYF_4$:Er@$NaYF_4$@$NaYF_4$:Yb/Tm@$NaYF_4$ nanoparticles were first synthesized to allow for dual-channel excitations (Figure 1b). By tuning the shell thickness of the $NaYF_4$:Yb/Tm layer, we obtained power-independent orthogonal luminescence (UV emission of Tm^{3+} under 980 nm excitation and green emission of Er^{3+} under 1532 nm excitation) with a high spectral purity, which was further utilized to enable reversible processing of data recording and erasing.

In our design, a layer-by-layer epitaxial growth procedure was adopted to introduce different activators into specific layers at precisely defined concentrations (Figures S1 and S2 and Scheme S1, Supporting Information). For orthogonal upconversion to proceed in favor of a precisely controlled photoreaction of DTE, Er^{3+}

Dr. K. Zheng, Dr. S. Han, Dr. X. Zeng, Y. Wu, Prof. X. Liu
Department of Chemistry
National University of Singapore
Singapore 117543, Singapore
E-mail: chmlx@nus.edu.sg
Dr. K. Zheng
State Key Laboratory on Integrated Optoelectronics
College of Electronic Science and Engineering
Jilin University
Changchun 130012, China
Prof. S. Song, Prof. H. Zhang
State Key Laboratory of Rare Earth Resource Utilization
Changchun Institute of Applied Chemistry
Chinese Academy of Sciences
Changchun 130022, China
E-mail: hongjie@ciac.jl.cn
Prof. X. Liu
Center for Functional Materials
National University of Singapore Suzhou Research Institute
Suzhou, Jiangsu 215123, China

The ORCID identification number(s) for the author(s) of this article can be found under https://doi.org/10.1002/adma.201801726.

DOI: 10.1002/adma.201801726

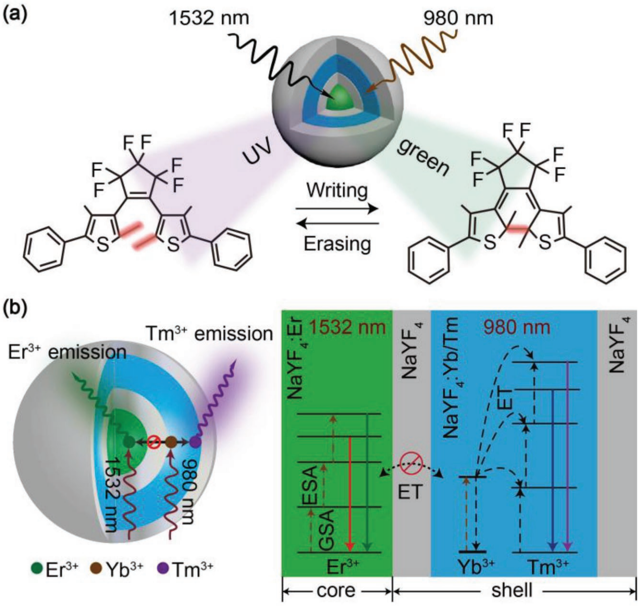

Figure 1. a) Schematic illustration of rewritable optical memory using core–shell upconversion nanoparticles combined with diarylethene molecules. The ultraviolet emission of the nanoparticles upon 980 nm excitation can be used to activate the cyclization reaction of DTE, while the green emission from the nanoparticles under 1532 nm irradiation can lead to the reversal ring-closure reaction of the DTE molecule. b) Schematic compositional layout (left) of the core–shell nanoparticle and proposed energy transfer pathways (right) between the lanthanide dopants under 980 and 1532 nm excitation, respectively.

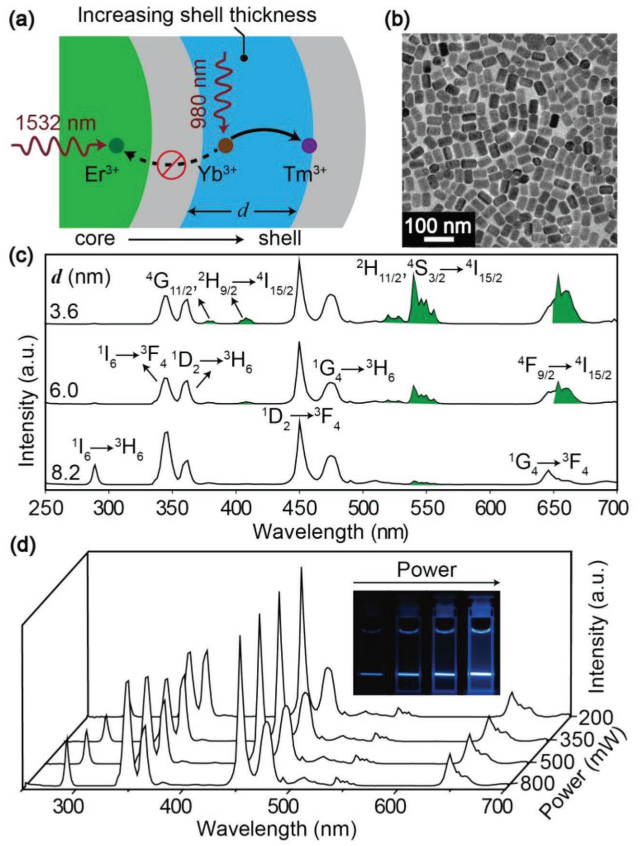

Figure 2. a) Schema representation of dual-channel orthogonal upconversion through shell thickness tuning. Four-tier from left to right refers to $NaYF_4$:Er, $NaYF_4$, $NaYF_4$:Yb/Tm, and $NaYF_4$ layer, respectively. b) Representative TEM image of the as-synthesized nanoparticles. c) Upconversion emission spectra of $NaYF_4$:Er@$NaYF_4$@$NaYF_4$:Yb/Tm@$NaYF_4$ nanoparticles as a function of $NaYF_4$:Yb/Tm shell thickness upon 980 nm excitation. d) Pumping power-dependent emission spectra of the as-synthesized nanoparticles by 980 nm excitation and the corresponding luminescence photographs (inset). Note that the emission spectra in (c) and (d) are normalized to Tm^{3+} 450 nm emission.

was confined in the core for generating green emission under 1532 nm excitation,[39–43] while Yb^{3+} and Tm^{3+} were codoped into the shell layer to enable UV emission under 980 nm excitation (Figure S3, Supporting Information). To prevent the energy transfer (ET) from Yb^{3+} to Er^{3+} and restrain the cross-relaxation of the excitation energy between Er^{3+} and Tm^{3+}, we further introduced an inert interlayer of $NaYF_4$ between the core and $NaYF_4$:Yb/Tm shell layer. Similarly, the $NaYF_4$ coating at the outermost layer of the nanoparticles was applied in order to eliminate the surface-related quenching of luminescence (Figure 1b).

It is important to note that Er^{3+} ion has an absorption band around 980 nm (Figure S4, Supporting Information).[44–47] To attain the proposed orthogonal upconversion, one must cut off the pathway of 980 nm photons to the Er^{3+} ions doped in the particle's core. We hypothesized that a heavy doping of Yb^{3+} ions in $NaYF_4$:Yb/Tm shell may prevent the 980 nm photons from reaching Er^{3+} in the core region because of a strong absorption of Yb^{3+}.

To validate our hypothesis, we prepared three batches of core–shell nanoparticles with different thicknesses (3.6, 6.0, 8.2 nm) of $NaYF_4$:Yb/Tm shell layer (**Figure 2**a; Figures S5–S7, Supporting Information). Transmission electron microscopy (TEM) of the samples showed a rod-like shape (Figure 2b). The crystalline nature and hexagonal-phased structure of the as-prepared nanoparticles were further confirmed by high-resolution TEM imaging and the corresponding Fourier transform pattern (Figure S8, Supporting Information). Photoluminescence study revealed that on 980 nm excitation the emission of Er^{3+} doped in the core decreases in intensity with increasing shell thickness of $NaYF_4$:Yb/Tm and the corresponding emission color of the particles changes from cyan to blue (Figure 2c; Figure S9, Supporting Information). Notably, a negligible emission peak (<1%) from Er^{3+} ions around 545 nm was detected when a 8.2 nm layer of $NaYF_4$:Yb/Tm was coated onto the $NaYF_4$:Er@$NaYF_4$ nanoparticles (Figure S10, Supporting Information). This can be explained by considering the fact that most of the 980 nm photons for excitation are consumed by Yb^{3+} absorption in the shell, leading to inadequate excitation of Er^{3+} ions in the core. Therefore, only Tm^{3+} emission was observed upon 980 nm excitation. In addition, with the excitation of different pumping power, the upconversion nanoparticles retained their spectral purity and emission color (Figure 2d; Figure S11, Supporting Information). Strikingly, upon switching the excitation wavelength to 1532 nm, the as-synthesized nanoparticles emitted green-yellow color, which can be attributed to the Er^{3+} emission (**Figure 3**a, top spectrum; Figure S12, Supporting Information). Taken together, these results illustrate that, in our

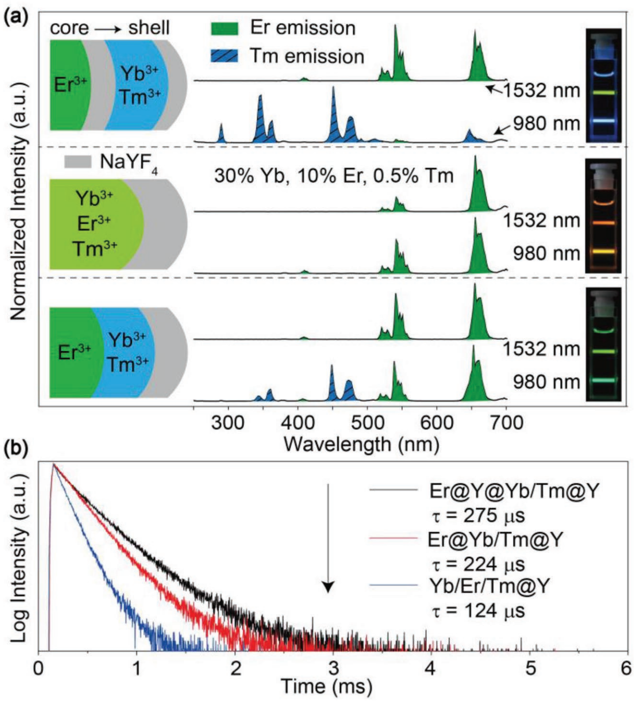

Figure 3. a) Upconversion luminescence profiles of $NaYF_4$:Er@$NaYF_4$@$NaYF_4$:Yb/Tm@$NaYF_4$, $NaYF_4$:Yb/Er/Tm@$NaYF_4$, and $NaYF_4$:Er@$NaYF_4$:Yb/Tm@$NaYF_4$ nanoparticles upon excitation at 980 and 1532 nm, respectively. Insets: schematic designs of the corresponding nanostructures (left); typical photographs taken from cyclohexane solutions of the nanoparticles under irradiation by two laser beams at wavelengths of 980 and 1532 nm (right). b) A comparison of luminescence lifetimes of Yb^{3+} in the nanocrystals with different structures, as shown in (a). The excitation and emission wavelength were fixed at 980 and 1000 nm, respectively.

particle system, a thick $NaYF_4$:Yb/Tm shell supports orthogonal upconversion with high spectral purity.

To shed more light on the multilayer design for achieving orthogonal emission, we carried out two control experiments. When the lanthanide activators (Er^{3+} and Tm^{3+}) were homogeneously doped with Yb^{3+} in the core, upconversion emissions from Tm^{3+} disappeared entirely with a 980 nm laser excitation (Figure 3a, middle spectrum). This is likely due to a much less doping concentration of Tm^{3+} (0.5 mol%) than that of Er^{3+} (10 mol%) in the codoped nanoparticles. In the case of $NaYF_4$:Er@$NaYF_4$:Yb/Tm@$NaYF_4$ nanoparticles, we observed both Er^{3+} and Tm^{3+} emissions on 980 nm excitation, although Er^{3+} ions were doped into a separate layer (core) from Yb^{3+} (Figure 3a, bottom spectrum). We believe that the Er^{3+} emission is mainly a result of dominant interfacial energy transfer from excited Yb^{3+} ions, in addition to the ground state absorption and excited state absorption processes. In stark contrast, the addition of an inert inner shell of $NaYF_4$ is able to block energy transfer (Yb → Er and Tm → Er) between the two neighboring layers, as evidenced by time-resolved photoluminescence studies (Figure 3b; Figure S13, Supporting Information). The inert inner $NaYF_4$ shell layer thus effectively promotes Tm^{3+} emission while concurrently suppressing Er^{3+} emission under 980 nm excitation. As a result, power-independent orthogonal upconversion of the $NaYF_4$:Er@$NaYF_4$@$NaYF_4$:Yb/Tm@$NaYF_4$ nanoparticles was achievable simply by switching the excitation wavelength from 980 to 1532 nm (Figure 3a, top spectrum; Figures S14 and S15, Supporting Information).

The ability of our multilayered nanoparticles to emit orthogonal luminescence on demand in response to NIR excitation wavelength provides a feasible way of triggering reversible photochemical reactions. As a proof of concept, we prepared a UCNP-DTE hybrid system for demonstration of rewritable optical memory application (Scheme S2, Supporting Information). Owing to the spectral overlapping between the absorption band of DTE molecules and the particle's upconversion emission, 980 and 1532 nm NIR irradiation can be used to direct the photochemical reaction from ring-opening to ring-closing (**Figure 4**a; Figure S16, Supporting Information). As shown in Figure 4b, upon irradiation of a 980 nm laser, the UV emission of Tm^{3+} facilitated the structural transformation of the DTE molecule from open to closed form, as accompanied by a color change in solution (Figures S17 and S18, Supporting Information).

By monitoring the time-dependent absorbance of DTE molecules at 570 nm, we found that the photostationary state was reached within 2 min under 980 nm excitation (Figure 4b). Similarly, the reverse ring-opening reaction of DTE molecules could be controlled using a 1532 nm laser, by which the purple solution gradually turned back to colorless with a decreased absorbance of DTE molecules at 570 nm (Figure 4b; Figure S18, Supporting Information). On the basis of luminescence dynamic studies, the induction of the DTE isomerization should be mainly attributed to radiation reabsorption instead of Förster resonance energy transfer (Figure S19, Supporting Information). By comparison, without the upconversion nanoparticles, no photocyclization reaction of pure DTE molecules could be implemented using an NIR laser (Figure S20, Supporting Information), indicating that the isomerization of DTE molecules is indeed induced by the emission of Er^{3+} and Tm^{3+} (Figures S21 and S22, Supporting Information). Importantly, our UCNP-DTE hybrid system exhibited good durability and no obvious degradation could be observed after several writing/erasing cycles (Figure S23, Supporting Information). To demonstrate the feasibility of our system in rewritable data storage, we prepared a thin film made of mixed UCNPs, DTE molecules and polymethyl methacrylate (PMMA), and subsequently performed time-dependent optical writing and erasing through optical microscopic lithography (Figure 4c; Figure S24, Supporting Information). As expected, an optical data point written onto the hybrid film through a 980 nm focused laser irradiation could be completely erased by switching the excitation wavelength to 1532 nm (Figure 4c). This capability further allowed us to continuously write, erase, and rewrite graphic optical data patterns on the same substrate (Figure 4d; Figure S25, Supporting Information). The specific data points recorded on the substrate could be readily replaced by a series of new data points with high registry through the upconversion-driven molecular editing process (Figure 4d; Figure S26, Supporting Information).

In conclusion, our experiments demonstrate that orthogonal upconversion emissions with high spectral purity can be achieved by core–shell crystal engineering, and that they

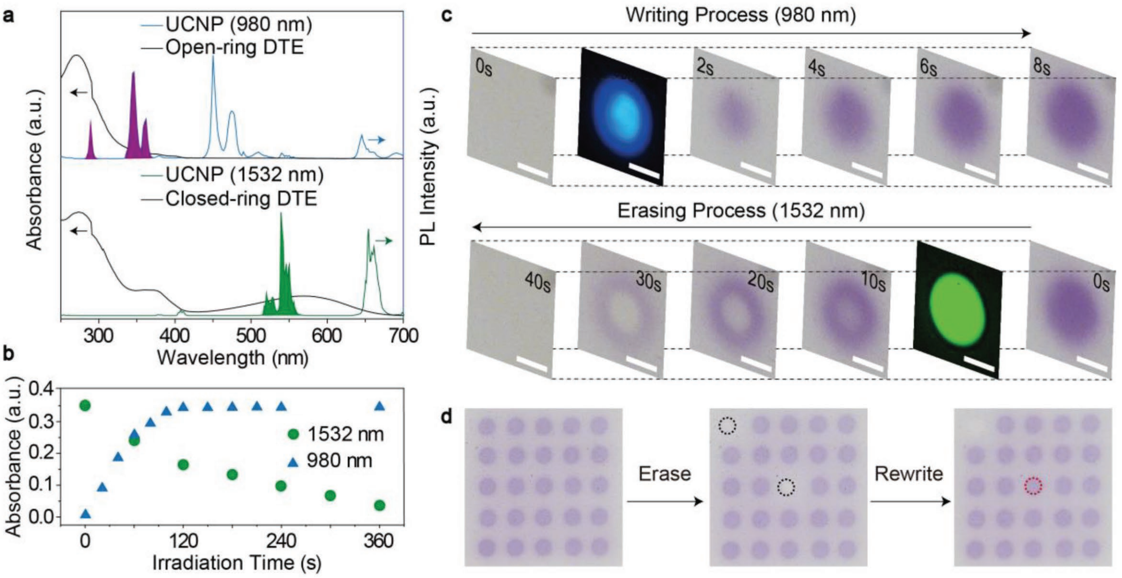

Figure 4. a) Upconversion emission spectra of the as-synthesized nanoparticles upon excitation at 980 and 1532 nm, respectively (Top panel: Tm^{3+} emission; bottom panel: Er^{3+} emission. The particle emissions overlap well with the absorption spectra of DTE molecules in both ring-opening and ring-closed form. b) Time-dependent absorbance changes of DTE molecules (20 µM) at 570 nm in chloroform solution in the presence of the nanoparticles (2 wt%) under 980 and 1532 nm excitation, respectively. c) Images showing time-dependent color changes (for date writing and erasing process, respectively) of a PMMA film containing a hybrid of UCNP-DTE upon excitation at 980 and 1532 nm, respectively. Scale bars: 50 µm. d) Demonstration of erasable and rewritable optical memory from a “5 × 5” pattern.

allow light-driven molecular editing to be precisely controlled. Notably, we have shown that multilayered $NaYF_4$ nanoparticles codoped with Er^{3+} and Tm^{3+} activators at different layers are capable of dual-channel orthogonal-upconversion luminescence on a single-particle level upon excitation at 980 and 1532 nm. This attribute enables to activate a DTE molecule-based reversible photochemical reaction, made possible by the introduction of phototransducers for orthogonal UV–vis radiation as well as subsequent energy transfer to the DTE molecules. The ability to selectively pump Er^{3+} or Tm^{3+} by a 1532 or 980 nm laser makes it possible to obtain high purity emission of Er^{3+} or Tm^{3+} for rewritable optical data storage. With the high registry of optical writing and erasing factored in, this approach could also lead to new techniques of manipulating and controlling electronic devices with NIR light.

Experimental Section

The experimental details are provided in the Supporting Information.

Supporting Information

Supporting Information is available from the Wiley Online Library or from the author.

Acknowledgements

This work was supported by the Singapore Ministry of Education (Grant Nos. R143000627112 and R143000642112), the National Research Foundation, Prime Minister’s Office, Singapore under its Competitive Research Program (CRP Award No. NRF-CRP15-2015-03), the National Basic Research Program of China (973 Program, Grant 2015CB932200), the National Natural Science Foundation of China (11774133, 21771135, 21471109, 21210001, and 21701119), and the CAS/SAFEA International Partnership Program for Creative Research Teams.

Conflict of Interest

The authors declare no conflict of interest.

Keywords

cyclization reaction, high spectral purity, optical memory, orthogonal upconversion, reversible photoswitching

Received: March 17, 2018
Revised: April 14, 2018

---

[1] J. A. Delaire, K. Nakatani, *Chem. Rev.* **2000**, *100*, 1817.
[2] F. M. Raymo, M. Tomasulo, *Chem. Soc. Rev.* **2005**, *34*, 327.
[3] S. Kawata, Y. Kawata, *Chem. Rev.* **2000**, *100*, 1777.
[4] D. Dulić, S. J. van der Molen, T. Kudernac, H. T. Jonkman, J. J. D. de Jong, T. N. Bowden, J. van Esch, B. L. Feringa, B. J. van Wees, *Phys. Rev. Lett.* **2003**, *91*, 207402.
[5] A. Peters, N. R. Branda, *J. Am. Chem. Soc.* **2003**, *125*, 3404.
[6] H. Tian, S. Yang, *Chem. Soc. Rev.* **2004**, *33*, 85.
[7] O. Nevskyi, D. Sysoiev, A. Oppermann, T. Huhn, D. Wöll, *Angew. Chem., Int. Ed.* **2016**, *55*, 12698.
[8] D. Kim, H. Jeong, H. Lee, W. T. Hwang, J. Wolf, E. Scheer, T. Huhn, H. Jeong, T. Lee, *Adv. Mater.* **2014**, *26*, 3968.

[9] M. Irie, T. Fukaminato, T. Sasaki, N. Tamai, T. Kawai, *Nature* **2002**, *420*, 759.
[10] V. W. W. Yam, J. K. W. Lee, C. C. Ko, N. Zhu, *J. Am. Chem. Soc.* **2009**, *131*, 912.
[11] C. C. Corredor, Z. Huang, K. D. Belfield, *Adv. Mater.* **2006**, *18*, 2910.
[12] D. Kitagawa, H. Nishi, S. Kobatake, *Angew. Chem., Int. Ed.* **2013**, *52*, 9320.
[13] F. Luo, C. Fan, M. Luo, X. Wu, Y. Zhu, S. Pu, W. Xu, G. Guo, *Angew. Chem., Int. Ed.* **2014**, *53*, 9298.
[14] D. J. Gargas, E. M. Chan, A. D. Ostrowski, S. Aloni, M. Virginia, P. Altoe, E. S. Barnard, B. Sanii, J. J. Urban, D. J. Milliron, B. E. Cohen, P. James Schuck, *Nat. Nanotechnol.* **2014**, *9*, 300.
[15] J. Hao, Y. Zhang, X. Wei, *Angew. Chem., Int. Ed.* **2011**, *50*, 6876.
[16] M. Haase, H. Schäfer, *Angew. Chem., Int. Ed.* **2011**, *50*, 5808.
[17] H. Dong, L. Sun, L. Li, R. Si, R. Liu, C. Yan, *J. Am. Chem. Soc.* **2017**, *139*, 18492.
[18] W. Zheng, P. Huang, D. Tu, E. Ma, H. Zhu, X. Chen, *Chem. Soc. Rev.* **2015**, *44*, 1379.
[19] N. J. J. Johnson, A. Korinek, C. Dong, F. C. J. M. van Veggel, *J. Am. Chem. Soc.* **2012**, *134*, 11068.
[20] Y. Liu, X. Yang, X. Zheng, S. Wen, F. Wang, X. Vidal, J. Zhao, D. Liu, Z. Zhou, C. Ma, J. Zhou, J. A. Piper, P. Xi, D. Jin, *Nature* **2017**, *543*, 229.
[21] C. D. Brites, X. Xie, M. L. Debasu, X. Qin, R. Chen, W. Huang, J. Rocha, X. Liu, L. D. Carlos, *Nat. Nanotechnol.* **2016**, *11*, 851.
[22] S. H. Nam, Y. M. Bae, Y. I. Park, J. H. Kim, H. M. Kim, J. S. Choi, K. T. Lee, T. Hyeon, Y. D. Suh, *Angew. Chem., Int. Ed.* **2011**, *50*, 6093.
[23] S. Han, R. Deng, X. Xie, X. Liu, *Angew. Chem., Int. Ed.* **2014**, *53*, 11702.
[24] Z. Zhou, H. Hu, H. Yang, T. Yi, K. Huang, M. Yu, F. Li, C. Huang, *Chem. Commun.* **2008**, 4786.
[25] C. J. Carling, J. C. Boyer, N. R. Branda, *J. Am. Chem. Soc.* **2009**, *131*, 10838.
[26] C. Zhang, H. Zhou, L. Liao, W. Feng, W. Sun, Z. Li, C. Xu, C. Fang, L. Sun, Y. Zhang, C. Yan, *Adv. Mater.* **2010**, *22*, 633.
[27] B. Zhang, M. Frigoli, F. Angiuli, F. Vetrone, J. A. Capobianco, *Chem. Commun.* **2012**, *48*, 7244.
[28] J. C. Boyer, C. J. Carling, B. D. Gates, N. R. Branda, *J. Am. Chem. Soc.* **2010**, *132*, 15766.
[29] C. J. Carling, J. C. Boyer, N. R. Branda, *Org. Biomol. Chem.* **2012**, *10*, 6159.
[30] T. Wu, D. Wilson, N. R. Branda, *Chem. Mater.* **2014**, *26*, 4313.
[31] J. C. Boyer, C. J. Carling, S. Y. Chua, D. Wilson, B. Johnsen, D. Baillie, N. R. Branda, *Chem. Eur. J.* **2012**, *18*, 3122.
[32] T. Wu, J. C. Boyer, M. Barker, D. Wilson, N. R. Branda, *Chem. Mater.* **2013**, *25*, 2495.
[33] H. Wen, H. Zhu, X. Chen, T. Hung, B. Wang, G. Zhu, S. Yu, F. Wang, *Angew. Chem., Int. Ed.* **2013**, *52*, 13419.
[34] X. Li, Z. Guo, T. Zhao, Y. Lu, L. Zhou, D. Zhao, F. Zhang, *Angew. Chem., Int. Ed.* **2016**, *55*, 2464.
[35] R. Deng, F. Qin, R. Chen, W. Huang, M. Hong, X. Liu, *Nat. Nanotechnol.* **2015**, *10*, 237.
[36] J. Lai, Y. Zhang, N. Pasquale, K. B. Lee, *Angew. Chem., Int. Ed.* **2014**, *53*, 14419.
[37] L. Wang, H. Dong, Y. Li, R. Liu, Y. Wang, H. K. Bisoyi, L. Sun, C. Yan, Q. Li, *Adv. Mater.* **2015**, *27*, 2065.
[38] H. Dong, L. Sun, W. Feng, Y. Gu, F. Li, C. Yan, *ACS Nano* **2017**, *11*, 3289.
[39] G. Chen, T. Y. Ohulchanskyy, A. Kachynski, H. Ågren, P. N. Prasad, *ACS Nano* **2011**, *5*, 4981.
[40] E. Verhagen, L. Kuipers, A. Polman, *Nano. Lett.* **2007**, *7*, 334.
[41] P. Chen, S. Yu, B. Xu, J. Wang, X. Sang, X. Liu, J. Qiu, *Mater. Lett.* **2014**, *128*, 299.
[42] Q. Chen, X. Xie, B. Huang, L. Liang, S. Han, Z. Yi, Y. Wang, Y. Li, D. Fan, L. Huang, X. Liu, *Angew. Chem., Int. Ed.* **2017**, *56*, 7605.
[43] S. Ivanova, F. Pellé, *J. Opt. Soc. B* **2009**, *29*, 1930.
[44] J. Zuo, Q. Li, B. Xue, C. Li, Y. Chang, Y. Zhang, X. Liu, L. Tu, H. Zhang, X. Kong, *Nanoscale* **2017**, *9*, 7941.
[45] N. J. J. Johnson, S. He, S. Diao, E. M. Chan, H. Dai, A. Almutairi, *J. Am. Chem. Soc.* **2017**, *139*, 3275.
[46] G. Tessitore, A. V. Mudring, K. W. Krämer, *J. Lumin.* **2017**, *189*, 91.
[47] H. Wang, Z. Yi, L. Rao, H. Liu, S. Zeng, *J. Mater. Chem. C* **2013**, *1*, 5520.